Control Algorithms for Plants Operating Under Variable Conditions, Applications

Stefan Preitl[1], Radu-Emil Precup[1], Zsuzsa Preitl[2], Alexandra-Iulia Stînean[1], Mircea-Bogdan Rădac[1], and Claudia-Adina Dragoş[1]

[1] Politehnica University Timisoara
Department of Automation and Applied Informatics
Bd. V. Parvan 2, RO-300223 Timisoara, Romania
{stefan.preitl,radu.precup,mircea.radac,claudia.dragos}@aut.upt.ro,
kassandra3107@yahoo.com
[2] Siemens AG, Erlangen, Germany (former at Politehnica University Timisoara and at Budapest University of Technology and Economics)
zsuzsap@yahoo.com

Abstract. The chapter deals with development, analysis and applicability of several easy applicable control algorithms, dedicated to plants working under continuously variable conditions: variable plant parameters or (the worst case) variable structure, variable reference and variable load (disturbance). Two speed control applications are selected and treated from the wide range of such applications: a case specific to the metallurgical industry, and the speed control of an electric (hybrid) vehicle model. The efficiency of the algorithms is tested and illustrated on different plant models and also on laboratory equipment with variable moment of inertia. The presented algorithms are easily adaptable to similar applications.

Keywords: Control algorithms, electrical driving systems, variable conditions, mathematical models, switching logic.

1 Introduction

Many industrial and non-industrial control applications are dedicated to plants working under continuously variable conditions, e.g., variable parameters and/or structure, variable reference and variable load disturbance, conditions which depends on the plant evolution. Representative applications are the domains of drives, i.e., electrical, hydraulic, pneumatic driving systems and thermal systems according to the examples given in [1–7].

Many theoretical and practical aspects may be solved in order to improve the control system performance expressed as performance specifications such as zero control error, robustness, good transients and disturbance rejection. For example:

1. The continuous variability of the inputs and parameters and the presence of the nonlinearities;

J. Fodor and R. Fullér (eds.), *Advances in Soft Computing, Intelligent Robotics and Control,* Topics in Intelligent Engineering and Informatics 8,
DOI: 10.1007/978-3-319-05945-7_1,

2. The presence of elasticity in power transfer (mechanical, for example) and derived, working in resonant regimes and suppress the oscillations, a notch filter may be inserted in the controller's structure [3, 5];
3. Complex optimization aspects in energy management [8, 9];
4. The presence of system noise and of actuating limits which reduce the control effect and the effect of the AWR measure, where the use of trajectory reference compensator and the mixing the effect of different modern control algorithms can ensure better robustness and control performances [2].
5. Nonlinearities in basic physical laws, for example, of the thermoelectric effects reflected, e.g., in Stefan-Boltzmann's law [10], etc.

Using the fact that in many applications relatively good models of the plant can be available, many theoretical, technical and practical control solutions can be developed and implemented as model-based control (MBC) solutions [2, 11–18] offering good control system performance.

Regarding the main idea, the control of plants working under continuously variable conditions, the chapter treats some easy applicable control algorithms. These algorithms are based on an output control strategy and tested on two class of application, on a laboratory equipments and/or simulation on detailed mathe-matical models of the plant.

The controlled plants are presented using relatively detailed Mathematical Models (MMs): the electrical driving system for an electric (hybrid) vehicle (EHV), for which the moment of inertia is relatively constant for a drive cycle, and a drive system with continuously Variable Moment of Inertia (VMI). Both plants have continuously variable inputs (reference and disturbance). Both applications are connected to drives with BLDC motors (BLDC-ms) or, particularly, with DC motors (DC-ms), using Cascade Control Structures (CCSs).

2 Practical Control Structures and Algorithms, Development Aspects for Plants Working Under Continuously Variable Conditions

A set of control algorithms (c.a.s) will be presented as follows as output control strategies. A part of the c.a.s is based on a single control loop and another one is based on the CCs. The analysed structures make use of an optimised inner (current) control loop. Therefore, the main control task, namely the speed control, is fulfilled by the main loop, by the speed controller which must be well designed.

2.1 The Classical Control Loop with PI(D) Controller

Due to the fact that the application is characterized mainly by continuously variable parameters in a relatively large domain, the control solution with bump-less switching of the c.a. can be a good, practical and relatively easily to implement option. The structure of this control solution is given in Fig. 1.

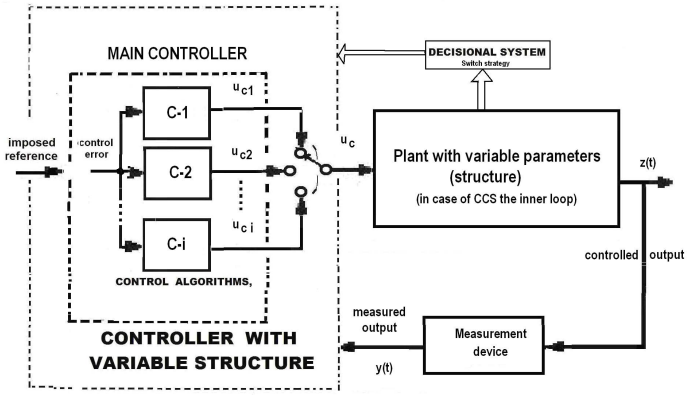

Fig. 1. The CCS with a switching logic for a speed controller

If the parameters of the plant are continuously variable and, as a consequence, the model can be easily linearised, the main aim of the designer is to bring the model in a benchmark type form [11]. Therefore, the design using classical or derived PI(D) control structures, becomes very convenient, and switching c.a.s are usable.

For example the switching structure for the classical PI controller with the transfer function (t.f.).

$$H_C(s) = \frac{k_c}{s}\left(1 + sT_c\right) = \frac{k_C}{sT_i}\left(1 + sT_i\right), \tag{1}$$

is presented in Fig. 2, and the corresponding digital c.a. has the form

$$\begin{aligned} u_{jk} &= -\frac{p_{1pi}^{(j)}}{p_{0pi}^{(j)}} \cdot u_{j,k-1} + \frac{q_{1pi}^{(j)}}{p_{0pi}^{(j)}} \cdot e_{j,k-1} + \frac{q_{0pi}^{(j)}}{p_{0pi}^{(j)}} \cdot e_{jk}, \\ j &= 1, 2, 3 \text{ c.a.}(j), \qquad e_{jk} = e_k \end{aligned} \tag{2}$$

with the parameters given by

$$\begin{aligned} q_{0pi} &= k_C + \frac{k_C T_e}{2T_i}, \quad & q_{1pi} &= -\left(k_C - \frac{k_C T_e}{2T_i}\right), \\ p_{0pi} &= 1, & p_{1pi} &= -1. \end{aligned} \tag{3}$$

In the cases of the considered applications, both of them as electrical driving systems, the design methods due to Kessler (the Modulus-Optimum method, MO-m and the Symmetrical Optimum method, SO-m synthesized in [11]) and various extensions derived from them are strongly recommended. Some remarkable extensions have been proposed by different authors: the Extended

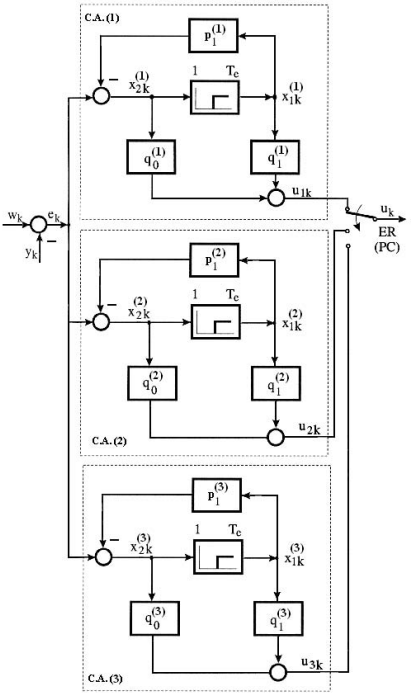

Fig. 2. Detailed block diagram of controller switching

Symmetrical Optimum method, ESO-m [17], the double parameterization based Symmetrical Optimum method, 2-p-SO-m given in [9] and also synthesized in [59], and [18–23, 27], etc. Moreover, the use of controllers with non-homogenous structure allows the construction of different forms of 2-DOF PI(D) structures [25–27] (Fig. 3).

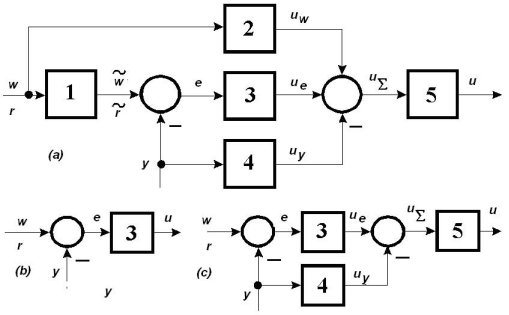

Fig. 3. Typical classical controller structures with extensions (basis for 2-DOF PI(D) controllers)

Due to the modifications of plant parameters, modifications in the c.a. must be included in different forms. Therefore, the controllers with switching can be considered as adaptive. They should have the benefit of taking into account such variations and retune its parameters. The switching structure is presented for the classical discrete PI c.a., but it can represent also other derived structures. Illustrative examples can be the Takagi-Sugeno PI type fuzzy controllers, the classical 2-DOF controllers, etc.

Beside the classical PI controller, the next section will consider the main controller in extended forms of 2-DOF and 2-DOF-PI(D) controllers, a PI Takagi-Sugeno Fuzzy Controller, a PI Quasi-Relay Sliding Mode controller and a Neuro-Fuzzy controller. The theoretical support for the controller design has been reported by the authors in terms of different forms. All solutions are based on the locally linearised MMs.

2.2 The Classical 2-DOF Control Loop and Extensions to 2-DOF PI(D) Controllers

The Basic structure. Polynomial design technique. The Control Structure (CS) with a 2-DOF controller uses two distinct controllers, Fig. 4, where (1) the reference filter with discrete t.f. $T(z)$ and (2) the feedback controller with discrete t.f. $S(z)$. The common part is represented by the discrete t.f. $R(z)$, which include the integral components of the controller.

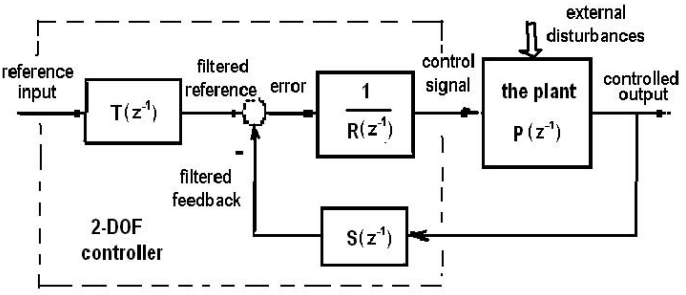

Fig. 4. Structure of the classical 2-DOF controller and control structure

In opposite with an one Degree of Freedom controller (1-DOF), in case of the 2-DOF controller structure, the enlisted requirements (Section 2.1) can be separately adjusted without influencing one another. The pragmatic design technique seat of the solution of a polynomial Diophantine equation, with different

particularities in treating constrains [9, 29, 32]. Supposing the plant characterised with the pulse transfer function (t.f.) calculated from the continuous model:

$$\begin{aligned} P(z) &= \left(1 - z^{-1}\right) Z\left\{\frac{P(s)}{s}\right\} \quad \text{and} \\ \frac{B(z)T(z)}{A(z)R(z) + B(z)S(z)} &= \frac{B_m(z)}{A_m(z)} \frac{A_0(z)}{A_0(z)}, \end{aligned} \tag{4}$$

where the servo performance specifications are imposed by a reference model in the form $B_m(z)/A_m(z)$, $T(z)$, $R(z)$, $S(z)$ are unknown polynomials; $A_m(z)$ determine the poles of the closed loop and $A_0(z)$ is the observer polynomial. Different causality conditions and degree conditions for the polynomials must be imposed in the development of the classical 2-DOF controller.

After accomplishing all operations, the final form of the Diophantine equation over the ring of polynomials is

$$A(z)R'(z) + B^-(z)S(z) = A_m(z)A_0(z) \tag{5}$$

having as solutions the coefficients of the $T(Z)$, $R(z)$, $S(z)$ polynomials. The polynomials $B^-(z)$ and $R'(z)$ in (5) are components of the factorized forms of $B(z)$ and $R(z)$ as follows:

$$B(z) = B^+(z)B^-(z) \quad \text{and} \quad B_m(z) = B^-(z)B'_m(z) \tag{6}$$

$$R(z) = B^+(z)R'(z) \quad \text{and} \quad R'(z) = (z-1)^1 R_1(z) \tag{7}$$

The $T(z)$, $R(z)$, $S(z)$ polynomials are finally obtained. Other development strategies are given in [31] and [36].

2-DOF PI(D) structures. Fig. 5 gives some particular structures derived from Fig. 3 [18, 25–27]. If the controllers presented in Fig. 5 are characterized by continuous t.f. with the tuning parameters $\{k_R, T_i, T_d, T_f\}$ [11], the expressions of $C(s)$ and $C_F(s)$ are [29]:

$$\begin{aligned} C(s) &= \frac{u(s)}{e(s)} = k_R \left(1 + \frac{1}{sT_i} + \frac{sT_d}{1 + sT_f}\right), \\ C_F(s) &= \frac{u_f(s)}{r(s)} = k_R \left(\alpha_1 + \alpha_2 \frac{sT_d}{1 + sT_f}\right). \end{aligned} \tag{8}$$

For the structure given in Fig. 5(b) (with the notation) the t.f.s are

$$\begin{aligned} C^*(s) &= \frac{u(s)}{e(s)} = k_R \left[(1 - \alpha_1) + \frac{1}{sT_i} + (1 - \alpha_2) \frac{sT_d}{1 + sT_f}\right], \\ C_P(s) &= \frac{u_f(s)}{r(s)} = k_R \left(\alpha_1 + \alpha_2 \frac{sT_d}{1 + sT_f}\right). \end{aligned} \tag{9}$$

Depending on the values of α_1 and α_2 (parameters), for the presented blocks the behaviours from in Table 1 are obtained. The choice of a certain representation of the controller depends on:

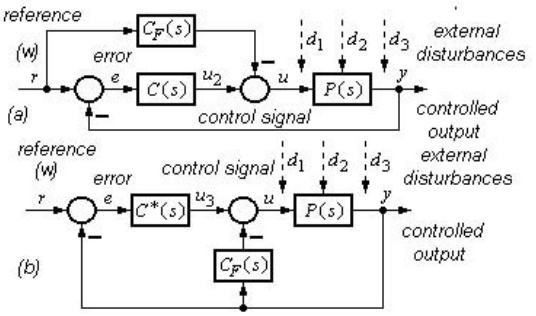

Fig. 5. Structures of 2-DOF PI(D) controllers as extension of an 1-DOF controller

1. The structure of the available controller;
2. The adopted algorithmic design method; and
3. The result of this design.

The table contains information regarding a possible extension with a reference filter $F(s)$.Other connections between 2-DOF and extended with input filters of 1-DOF controller structures are synthesized in [26, 29–31, 33], etc.

Table 1. Connections between 2-DOF controller and extended 1-DOF controller structure (P – proportional, D – derivative, I – integral, L1(2) – first (second) order filter with lag)

		$F(s)$	–	$F(s)C(s)$	$C(s)$	Remarks
Fig. 4(a)		–	C_F	$C(s) - C_F(s)$	$C(s)$	–
Fig. 4(b)		–	C_P	$C^*(s)$	$C^*(s) + C_P(s)$	–
α_1	α_2	–	–	(ref. channel)	(feedback)	
0	0	1	0	PID	PID	1-DOF controller
0	1	PDL2	DL1	PI	PID	1-DOF with non-
1	0	PD2L2	P	PID-L1	PID	homogenous behaviour
1	1	PL2	PDL2	I	PID	
α_1	α_2	PID controller with pre-filtering (2-DOF controller)				

2.3 Extensions to Fuzzy Controller Solutions. 2-DOF Takagi-Sugeno PI(D) Fuzzy Controllers

The Takagi-Sugeno PI quasi-continuous fuzzy controller structure (TS-PI-FC) with output integration (OI), Fig. 6, was adopted based on the continuous-time PI controller solution. The algorithm is modelled by the recurrent equations

with variable parameters; finally this leads to the PI quasi-continuous digital controller with output integration (OI) [30, 31, 36]:

$$\begin{aligned} \Delta u_k &= K_P \Delta e_k + K_i e_k = K_P \left(\Delta e_k + \alpha e_k\right), \\ K_P &= k_C \left(1 - \frac{T_e}{2T_i}\right), \quad K_i = \frac{k_C T_e}{T_i} \quad \alpha = \frac{K_i}{K_P} = \frac{2T_e}{2T_i - T_e}, \\ B_{\Delta e} &= \frac{K_i}{K_P} B_e, \quad B_{\Delta e} = \alpha B_e, \quad B_{\Delta u} = K_i B_e \end{aligned} \tag{10}$$

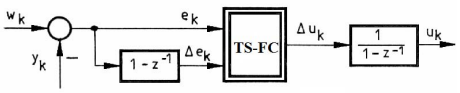

Fig. 6. TS-PI-FC (OI) structure with output integration

The TS-PI-FC is characterized by the following features:

(i) The fuzzification is performed by means of three membership functions $\{N, ZE, P\}$ pointing out the TS-PI-FC tuning parameters $\{B_e, B_{\Delta e}, B_{\Delta u}\}$;
(ii) The inference engine uses the SUM and PROD operators assisted by the rule base presented in Table 2 [3]; and
(iii) It employs the weighted average method for defuzzification.

Table 2. Rule base of TS-PI-Fuzzy Controller with Output Integration (also for Input Integration)

$\Delta e_k / e_k$	N	ZE	P
P	$K_{p1}[\Delta e_k + \alpha_1 e_k]$	$K_{p2}[\Delta e_k + \alpha_2 e_k]$	$K_{p3}[\Delta e_k + \alpha_3 e_k]$
ZE	$K_{p4}[\Delta e_k + \alpha_4 e_k]$	$K_{p5}[\Delta e_k + \alpha_5 e_k]$	$K_{p6}[\Delta e_k + \alpha_6 e_k]$
N	$K_{p7}[\Delta e_k + \alpha_7 e_k]$	$K_{p8}[\Delta e_k + \alpha_8 e_k]$	$K_{p9}[\Delta e_k + \alpha_9 e_k]$

The expressions of the c.a.s are

$$\begin{aligned} u_{jk} &= u_{j,k-1} + K_{Pi}^{(j)} \left[\left(1 - \alpha_i^{(j)}\right) e_{jk} - e_{j,k-1}\right], \quad i = 1, \ldots, 9 \\ e_{jk} &= w_k - y_k = e_k, \qquad\qquad\qquad\qquad j = 1, 2, 3 \text{ for the c.a.}(j) \end{aligned} \tag{11}$$

Extended 2-DOF PI(D) Fuzzy Control structures can be defined on the basis of the structures illustrated in Fig. 5 and 6. 2-DOF FCs are proposed in [30] and [31], and they are defined on the basis Takagi-Sugeno fuzzy blocks FB-Tc as illustrated in Figs. 7 to 10.

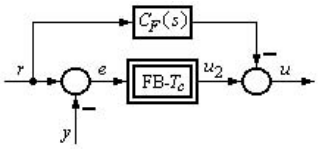

Fig. 7. Structure of feed-forward 2-DOF PI-fuzzy controller

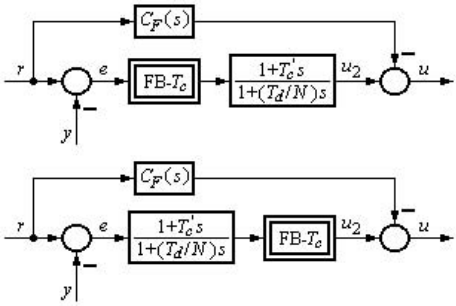

Fig. 8. Structures of feed-forward 2-DOF PID-fuzzy controllers

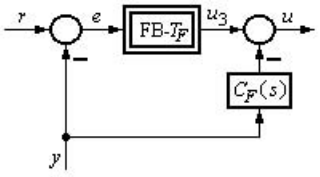

Fig. 9. Structure of feedback 2-DOF PI-fuzzy controller

To develop the PI(D)-FC, the continuous-time PI controllers must be expressed in one of its incremental PI quasi-continuous digital version (10), that leads to

$$\Delta u_{i,k} = K_{Pi}\Delta e_{i,k} = K_{Ii}\left(\Delta e_{i,k} + \delta_i e_{i,k}\right), \qquad i = \overline{1,2}, \tag{12}$$

where $\{K_{Pi}, K_{Ii}, \delta_i\}$ can be easily calculated from the continuous t.f. The rule bases of the two blocks FC_i can be expressed in terms of the decision table shown in Table 3, representing the consequent part of the inference rules.

The strictly positive parameters of the PI-FCs are $\{B_{ei}, B_{\Delta ei}, B_{\Delta ui}, m_i, n_i, p_i\}$ which are in correlation with the shapes of the input membership functions, Fig. 11, and the parameters m_i, n_i and p_i (Table 3), $m_i < n_i < p_i$, have been added to the standard version of PI-FCs to improve the CS performance by modifying the input-output static map of the blocks FC_i.

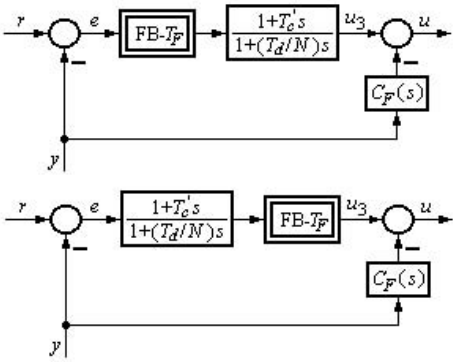

Fig. 10. Structures of feedback 2-DOF PID-fuzzy controller

Table 3. Decision Table of FCi, $i = \overline{1,2}$

$\Delta e_{i,k} \setminus e_{i,k}$	NB	NS	ZE	PS	PB
PB	$\Delta u_{i,k}$	$m_i\Delta u_{i,k}$	$n_i\Delta u_{i,k}$	$p_i\Delta u_{i,k}$	$p_i\Delta u_{i,k}$
PS	$m_i\Delta u_{i,k}$	$\Delta u_{i,k}$	$m_i\Delta u_{i,k}$	$n_i\Delta u_{i,k}$	$p_i\Delta u_{i,k}$
ZE	$n_i\Delta u_{i,k}$	$m_i\Delta u_{i,k}$	$\Delta u_{i,k}$	$m_i\Delta u_{i,k}$	$n_i\Delta u_{i,k}$
NS	$p_i\Delta u_{i,k}$	$n_i\Delta u_{i,k}$	$m_i\Delta u_{i,k}$	$\Delta u_{i,k}$	$m_i\Delta u_{i,k}$
NB	$p_i\Delta u_{i,k}$	$p_i\Delta u_{i,k}$	$n_i\Delta u_{i,k}$	$m_i\Delta u_{i,k}$	$\Delta u_{i,k}$

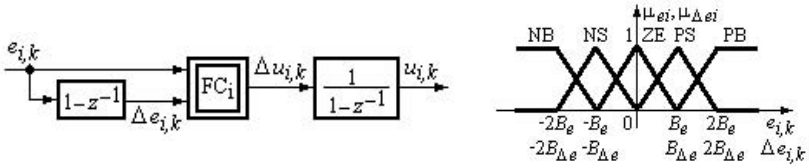

Fig. 11. The PI-FC structure and initial input membership functions of FC_i, $i = \overline{1,2}$

The development method dedicated to the two TS-PI-FCs consists of five steps detailed in [25, 33, 35].

Other TS-FC-based control solution for plants with time variable parameters – e.g. with VMI – are presented in [28, 34] where a Two Input-Single Output Takagi-Sugeno (TISO) Linear Time Variant (LTV) is used to model the controlled plant. Other applications are presented also in [37, 38].

2.4 The PI Quasi-Relay Sliding Mode Controller

The structure of a classical PI quasi relay sliding-mode controller with parameter adaptation is presented in Fig. 12. The design steps of the controller are presented as follows on the basis of mainly [12] and [17]:

(a) For the classical PI part. (i) The variable parameter T_i can be determined in terms of the pole-zero cancellation regarding the t.f. of the plant.
(b) For the sliding mode part. (ii) The positive parameter c is chosen taking into account the imposed performance: $c < a_2$, where a_2, a_1 and b are the parameters in Ackerman's form of the state-space representation of the plant model; (iii) The parameter α is calculated by taking into account the desired existence domain for the sliding mode control.

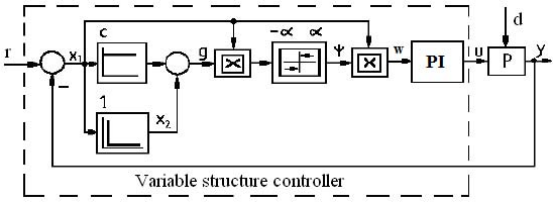

Fig. 12. The PI quasi relay sliding mode controller (the classical structure)

The control law is presented in its parallel form

$$\begin{aligned} u(t) &= \Psi(t)x_1(t) + \frac{1}{T_i}\int_0^t \Psi(\tau)x_1(\tau)\mathrm{d}\tau, \qquad x_1 = e, \\ \Psi(t) &= \alpha \,\mathrm{sgn}\left\{g(t)x_1(t)\right\}, \end{aligned} \tag{13}$$

where the parameter α is tuned in terms of

$$\alpha < \frac{-\left|\left(c^2 - a_2 c + a_1\right)x_1(t) - f(t)\right|}{|x_1(t)| + \frac{1}{T_i}\int_0^t x_1(\tau)\mathrm{d}\tau}. \tag{14}$$

The expressions and parameters of the digital c.a.s are similar to (10) and (11), having different values and with the expressions of the control algorithm also given in [24, 31, 40–43].

2.5 The Hybrid Neuro-Fuzzy TS PI Controller and the Design Approach

The presented structure of the extended fuzzy control system contains a hybrid Takagi-Sugeno PI-neuro-fuzzy controller (T-S PI-N-FC) [4] Fig. 13, where: AB is the adaptation block, RM is the reference model, r is the reference input, e_k

is the control error, k is the index of the current sampling interval, $k \in \mathbb{Z}$, and q^{-1} is the backward shift operator.

The parameter $B_{e,k}$ replaces the parameter B_e specific to the T-S PI-FC with Input Integration (-II) [3, 12, 17] given in Fig. 14. T-S FB is the nonlinear Takagi-Sugeno fuzzy block without dynamics; $e_{I,k}$ is the integral of control error e_k:

$$e_{Ik} = e_{I,k-1} + T_s e_k, \qquad T_k \text{ – the sampling period.} \tag{15}$$

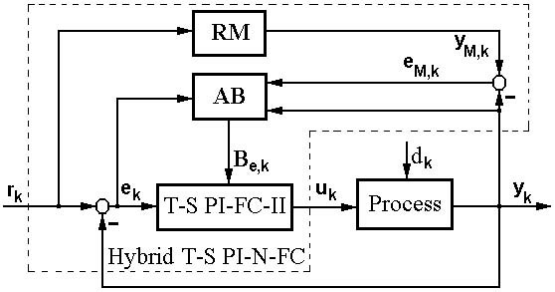

Fig. 13. Fuzzy control system structure with hybrid T-S PI-NF-C

T-S FB has the following features: (i) The fuzzification is carried out by means of the input membership functions presented in Fig. 14(b), which points out two tuning parameters, B_e and B_{eI}; (ii) It uses the SUM and PROD operators in the in-ference engine, and the weighted average method for defuzzification.

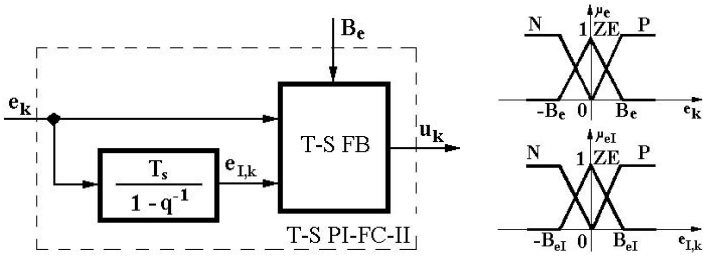

Fig. 14. Structure of T-S PI-FC-II and the input membership functions

The complete rule base of T-S PI-FC-II is formulated such that to ensure the combination of nine separately designed PI controllers with t.f.s given in (1) rewritten with superscripts:

$$H_C^m(s) = \frac{k_C^m}{sT_i^m}\left(1 + T_i^m s\right), \qquad m = 1, \ldots, 9. \tag{16}$$

Discretising (16), the quasi-continuous digital PI control algorithm results as

$$u_k^m = k_C^m e_k + \frac{k_C^m}{T_i^m} e_{I,k}, \qquad m = 1, \ldots, 9, \tag{17}$$

u_k^m is the control signal produced by the m^{th} PI algorithm, $m = 1, \ldots, 9$. The algorithms are introduced in the consequents of the rules of T-S PI-FC-II, expressed as

$$\begin{aligned} \text{Rule } m\text{:} \quad & \text{IF } e_k \text{ IS } LT_{m1} \text{ AND } e_{I,k} \text{ IS } LT_{m2} \\ & \text{THEN } u_k^m = k_C^m e_k + \frac{k_C^m}{T_i^m} e_{I,k}, \qquad m = 1, \ldots, 9, \end{aligned} \tag{18}$$

where $LT_{ml} \in \{N, ZE, P\}$, $m = 1, \ldots, 9$, $l \in \{1, 2\}$ are the input linguistic terms with the membership functions defined in Fig. 14(b). The modal equivalence principle [18] is applied and modified to obtain the covering of all input linguistic terms:

$$B_{eI} = \left(\min_{m=1\ldots9} T_i^m \right) B_e. \tag{19}$$

The parameter B_e is online adapted by the Model Reference Adaptive Control (MRAC) structure presented in Fig. 14 and is discussed in details in [56, 57]. Based on the (continuous) t.f., the RM block sets the CS performance specifications. The AB consists of a single unbiased neuron with a linear activation function, characterized by a recurrent equation that ensures the training in the framework of back propagation with momentum factor [56]:

$$\begin{aligned} w_k &= -\eta e_{M,k} \frac{\Delta y_k}{\Delta B_{e,k}} e_k + \lambda \Delta w_{k-1}, \\ w_k &= w_{k-1} + \Delta w_k, \\ B_{e,k} &= q_k e_k, \end{aligned} \tag{20}$$

where w_k is the input weight of the neuron, $0 \leq \eta \leq 1$ is the learning rate, and $0 \leq \lambda \leq 1$ is the momentum factor. More details regarding the design are presented in [56–58].

The design approach guarantees the stability of the fuzzy control system. The fuzzy control system dedicated to a class of servo systems with variable parameters ensures the behaviour of control systems with bump-less combinations of separately tuned linear PI controllers as shown in [23, 25, 30].

3 Examples of Electrical Driving Systems. Mathematical Models

In the symmetrical operating mode the Mathematical Models (MMs) of BLDC-ms and of classical DC-ms are very close [6, 7, 44–47]. That leads to similarities in the derived benchmark-type models used in development of control solutions.

Since the control of the main characteristic variables (speed and position) of servo drives with DC-m and BLDC-m is well-known and product on a large scale by industry such control solutions are characterized as LCA solutions. The inner loop (the current loop) can differ but it can be relatively easy optimized.

3.1 The Mathematical Model of a BLDC-m (Servo Drive)

The matrix form of the main equations of the MM of a BLDC-m is given in [6, 7, 44–47, 50]:

$$\begin{bmatrix} V_{AS} \\ V_{BS} \\ V_{CS} \end{bmatrix} = \begin{bmatrix} R_a & 0 & 0 \\ 0 & R_b & 0 \\ 0 & 0 & R_c \end{bmatrix} \begin{bmatrix} i_{as} \\ i_{bs} \\ i_{cs} \end{bmatrix} + \frac{\mathrm{d}}{\mathrm{d}t} \begin{bmatrix} L_a & L_{ab} & L_{ac} \\ L_{ba} & L_b & L_{bc} \\ L_{ca} & L_{cb} & L_c \end{bmatrix} \begin{bmatrix} i_{as} \\ i_{bs} \\ i_{cs} \end{bmatrix} + \begin{bmatrix} e_a \\ e_b \\ e_c \end{bmatrix}, \quad (21)$$

where: R_a, R_b, R_c and L_a, L_b, L_c – the resistance and the phase inductance, L_{ab}, L_{bc}, L_{ca} – the mutual (between phases) inductance, e_a, e_b, e_c – the electromotive voltage, V_{AS}, V_{BS}, V_{CS} and i_{as}, i_{bs}, i_{cs} – the phase voltages and currents. Based on it, the electromagnetic torque me of BLDC-m results as

$$m_e = \frac{e_a i_{as} + e_b i_{bs} + e_c i_{cs}}{\omega_r}. \quad (22)$$

The model for the mechanical part – the movement equation is well-known:

$$m_e = J_e \frac{\mathrm{d}}{\mathrm{d}t} \omega_r + k_f \omega_r + m_{\mathrm{Load}}, \quad (23)$$

where m_{Load} is the load torque (i.e., a time variable load-type disturbance) and the moment of inertia (constant or more generally, time variable) can be expressed as

$$J_e(t) = J_{\mathrm{BLDC}+J_{\mathrm{mech}}(t)}. \quad (24)$$

Based on functionality of the BLDC-m, the informational block diagram of a BLDC-m with permanent magnets is appropriate to the informational block diagram of the DC-m. A block diagram of a BLDC-m drive developed for the control purpose is represented in Fig. 14 [33]. This diagram is related to the detailed online switching scheme for the PWM converter illustrated in Fig. 15. Extensive control strategies for BLDC-m applications described in literature.

3.2 The Mathematical Model of an Electric HEV with DC-m (BLDC-m)

The traction and the optimization of fuel consumption for an electric vehicle (EV) (more generally, HEV) [9] consists in the electric driving system but can include extensions relative the primary energy sources [8, 9, 51]. The primary energy sources of these vehicles can be different:

1. Pure electrical sources, based on batteries;
2. Hybrid primary energy sources with different structures and components.

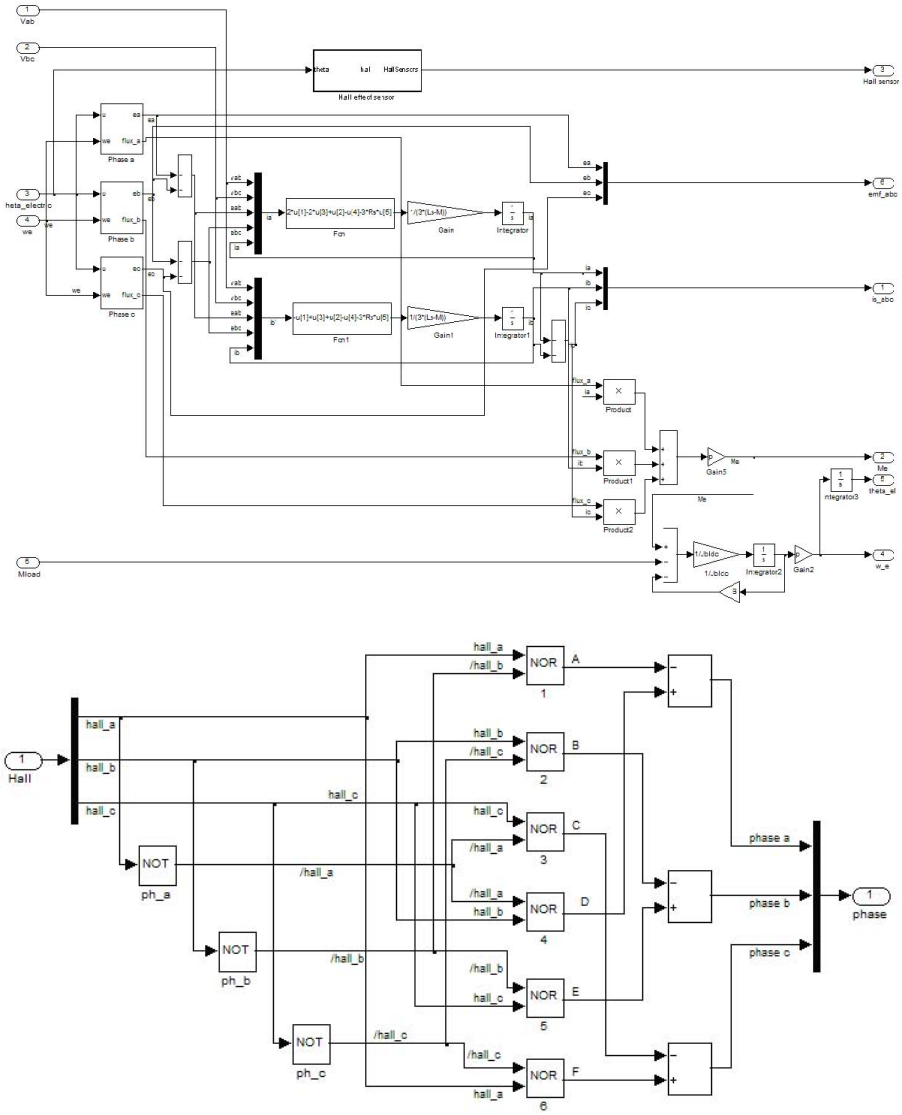

Fig. 15. The equivalent circuit of a BLDC-m control solution

In case of HEVs, the electrical machine, e.g., the DC-m or the BLDC-m, can work as a motor (traction regime) or as a generator (in regenerative braking regime). Considering the case of DC-m the functional block diagram of an electrical driving system as part of an HEV (EV) is presented in Fig. 16, and it offers support for detailed mathematical modelling [6, 7, 9, 48, 49].

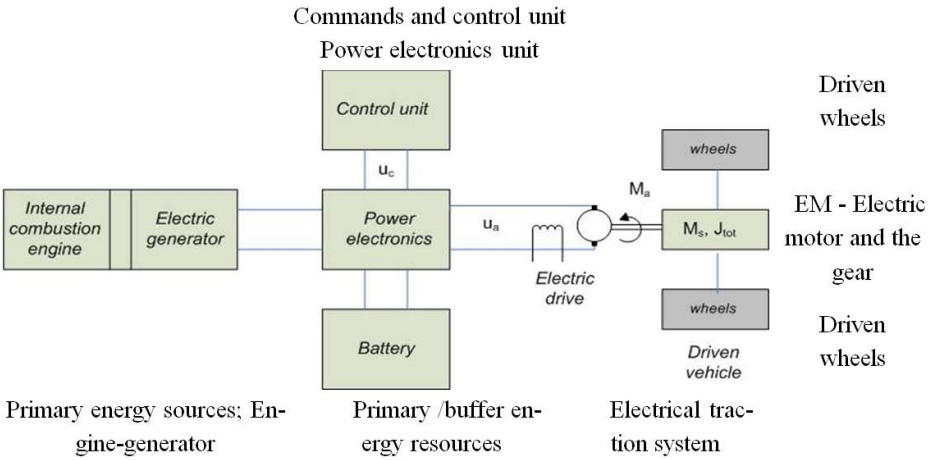

Fig. 16. Basic diagram of a hybrid electric vehicle

Vehicle Movement. The vehicle dynamics can be modelled using the basic dynamical relations for vehicle motion, considering also the rolling resistance, hill climbing and aerodynamic drag. The basic relations that describe the driven sys-tem consist of the simple longitudinal dynamics of the vehicle are

$$\omega(t) = \frac{f_r}{w_r} v(t), \qquad M_d(t) = \frac{w_r}{f_r} F_d(t), \tag{25}$$

$$F_d(t) = m\dot{v}(t) + \frac{1}{2}\rho v^2(t) A_d C_d + mg\big(\cos(\gamma(t))C_r + \sin(\gamma(t))\big). \tag{26}$$

where F_d is the drive force, m is the mass of vehicle, v is its velocity, ρ is the air density, A_d is the frontal area of the vehicle, C_d is the air drag coefficient, C_r is the rolling resistance coefficient, γ is the road rise angle, $M_d = M_s$ is the torque required from the EM, f_r is the final drive ratio, and w_r is the wheel radius.

Driving System with DC-m. The basic equations that characterize the functionality of the system are

$$\begin{aligned} L_a di_a + R_a i_a = u_a - e \quad \text{with} \quad u_a \approx k_A u_c, \qquad T_a = \frac{L_a}{R_a}, \\ e = k_e \omega, \qquad M_a = k_m i_a, \qquad M_d(t) = \frac{w_r}{f_r} F_d(t), \\ J_{\text{tot}0}\dot{\omega} = M_a - M_s - M_f, \qquad J_{\text{tot}} = J_m + J_{\text{veh}} + J_w, \end{aligned} \tag{27}$$

where the classical notations were used (in SI units). The inertia of the system can change with maximum +50% (in some cases much more) regarded to the basic value $J_{\text{tot}0}$, which corresponds to the vehicle without passengers, is

$$J_{\text{tot}} = J_{\text{tot}0} + \Delta J_t \quad \text{with} \quad \Delta J_t \le 0.50 J_{t0}. \tag{28}$$

Using equations (25)–(27), the block diagram of system can be built and based on it, the t.f. with respect to the control signal $H_{\omega,uc}(s)$ can be derived

$$H_{\omega,uc}(s) \approx k_A \frac{1/k_e}{(1+sT_a)(1+sT_m)} \quad \text{with} \quad T_m = \frac{J_{\text{tot}} R_a}{k_m k_e}, \tag{29}$$

where T_m is the mechanical time constant, and this form corresponds to a second order with lag benchmark type model.

Numerical data related to the application (as part of an HEV) are defined in [52] and used in [9] and presented in Table 4. Other electrical data (from the car builder): $R_a \approx 0.1\ \Omega$; $k_A = 30$ V/V, gain and time constant of actuator; $k_{Mi} = 0.0238$ V/A; $k_{M\omega} = 0.0178$ V/(rad/sec) gains for current and speed sensors.

Table 4. Numerical values for the DC-m

Torque [Nm]	Rotation [rot/min]	Usef.power [kw]	Voltage [V]	Current [A]	Nom.Power [kw]	Efficiency [%]	El.time const [sec]
50.16	1605	8.43	77.6	126	10.00	86.18	0.1

Numerical values regarded to the vehicle (from the car builder) [9]: total mass of vehicle, including an 80 kg heavy driver: $m_{\text{tot}} = 1860$ kg; frontal area of vehicle: $A_d = 2.4\ \text{m}^2$; air drag coefficient: $C_d = 0.4$; air density: $\rho = 1.225\ \text{kg/m}^3$; rolling resistance coefficient: $C_r = 0.015$; wheel radius: $w_r = 0.3$ m; final drive ratio: $f_r = 4.875$ Nm/(rad/sec). Using the energy conservation principle, the numerical value is

$$J_{\text{veh}} = 1860 \cdot \frac{0.3^2}{4.875^2} = 7.04\ \text{kg m}^2. \tag{30}$$

Let us consider the moment of inertia of the wheels and electric motor, J_W, then result the value of the total inertia J_{tot}:

$$J_W = 1.56\ \text{kg m}^2, \qquad J_{\text{tot}} = J_{\text{veh}} + J_W = 8.6\ \text{kg m}^2 \tag{31}$$

which is reflected in the mechanical time constant of the plant. For the two time constants are $T_m = 5.43$ sec and $T_a = 0.1$ sec resulting in a value of $m \approx 0.2$. This value can be used in controller design based on 2p-SO-m [9, 27].

3.3 Application with Variable Inputs and Variable Moment of Inertia

Some driving systems are characterized by variable inputs, VMI and coupled oscillating mechanisms. For such applications, the developer of a proper c.a. must solve three main problems:

1. The adequate modification of the reference input (ω_0);
2. The choice of a proper CS and tuning method for the controller for the plant working under the VMI conditions;
3. Attenuate the oscillations (this problem, solved in [3], is not treated in this chapter).

The treated example concerns the speed control of a winding system, Fig. 17, having a rigid connection in the driving part. In case of a winding process [33], the main conditions to be fulfilled by the control solutions are

$$\begin{aligned} v_t(t) = \text{const} \quad &\Rightarrow \quad \omega_0(t) = \frac{k}{r_t(t)}, \\ f_t(t) = \text{const}, \quad &\text{and} \quad J_e(t) = \frac{1}{2}\rho\pi l r^4(t). \end{aligned} \tag{32}$$

The continuous change of the reference $\omega_0(t)$ can be ensured on the basis of the radius $r(t)$. The speed control can be solved in various ways, for example:

1. Using a cascade CS with two loops - the current loop - and the speed loop (With, conventional or advance controller, see paragraph 4);
2. Using a state feedback CS and superpose and a Zero-Steady-state Error Controller.

The changing in a large domain of the equivalent moment of inertia $J_e(t)$, illustrated in Fig. 18, requires much attention in the controller design.

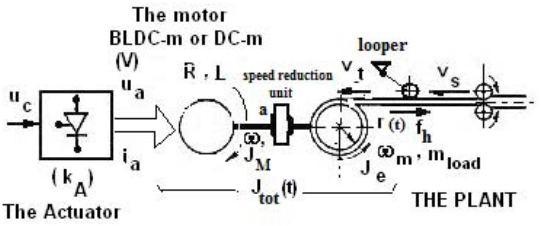

Fig. 17. Functional diagram of VIWP and reference input correction system

Neglecting the frictions, simplified but highly acceptable state-space MMs of the plant can be derived. Indifferent from the motor type (BLDC-m or DC-m), linearising the model at some representative operating points, the following simply input-output benchmark-type t.f.s can be obtained (see also (29)):

– in the speed control applications:

$$\begin{aligned} H_P(s) &= \frac{k_P}{(1+sT_\Sigma)(1+sT_1)} \quad \text{or} \\ H_P(s) &= \frac{k_P}{(1+sT_\Sigma)(1+sT_1)(1+sT_2)}, \end{aligned} \tag{33}$$

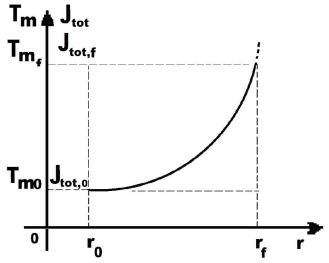

Fig. 18. The inertia and mechanical time constant variation as function of drum radius

– in the position control applications:

$$H_P(s) = \frac{k_P}{s\,(1 + sT_\Sigma)} \quad \text{or}$$
$$H_P(s) = \frac{k_P}{s\,(1 + sT_\Sigma)\,(1 + sT)}, \tag{34}$$

with $T_1 > T_2 \gg T_\Sigma$, but $T_1 = f(J_e(t))$ is/can be time-variable, Fig. 18.

If the variation range of $J_e(t)$ is relatively small the controller structure can be relatively simply; if the variation range of $J_e(t)$ is large, adaptive or variable structure controllers must be used [33]. However, the evaluation of the VMI ($J_e(t)$) can be a difficult task for the control designer. If the parameters changing $\{l, r(t), \rho\}$ are measurable, the problem has relatively easy solutions. If not, the changes in inertia can be evaluated using different estimation schemes; for example in [3], a relatively simple stable observer for a single-mass mechanical model of the plant is presented; more complex fuzzy model observers were developed and presented in literature.

The developed bump-less switching strategy in the controller structure (algorithm) (Figs. 1 and 2) is applicable without difficulties to both mentioned c.a.s, the classical PI(D) controller and the TS-FCs. The developed CSs are discussed considering two case studies (plants):

The simulated case that involves DC-m drive with VMI, characterized by the following parameters: rated voltage $u_{an} = 24\,\mathrm{V}$, rated current $i_{an} = 3.1\,\mathrm{A}$, rated speed $\omega = 3000\,\mathrm{rpm}$, rated torque $M_{e,n} = 0.15\,\mathrm{Nm}$, rotor inertia $J_m = 0.18 \cdot 10^{-4}\,\mathrm{kg\,m^2}$, terminal resistance $R_s = 2\,\Omega$, mechanical time constant $T_m = 0.013\,\mathrm{s}$, electrical time constant $T_a = 0.001\,\mathrm{s}$, torque constant $k_m = 0.056\,\mathrm{Nm/A}$. The increasing radius $r(t)$ determines an increase of the value of the total moment of inertia from $J_{\mathrm{tot},0} = 0.18 \cdot 10^{-4}\,\mathrm{kg\,m^2}$ to $J_{\mathrm{tot},f} = 1.372 \cdot 10^{-4}\,\mathrm{kg\,m^2}$, and corresponding, the increasing of the mechanical time constant T_m.

Laboratory application, with $J_e(t)$ variable "in steps"; the equipment Model 220 Industrial plant is presented in Fig. 19 [53]. The equipment allows for the realization of three different mechanical structures. The experiments have been conducted for different control structures and controllers, see Section 4.3. For this application, the numerical values of the parameters are synthesized in Table 5.

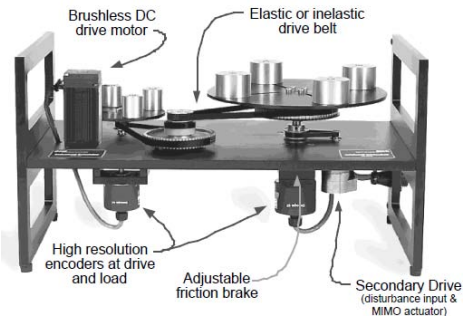

Fig. 19. Model 220 Industrial Plant Emulator (M 220 IPE)

Table 5. Numerical values for M 220 IPE

Parameters	Values of the parameters
J_{dd}	$0.00040\,\mathrm{kg\,m^2}$
J_{dl}	$0.0065\,\mathrm{kg\,m^2}$
J_{p_backlash}	$0.000031\,\mathrm{kg\,m^2}$
$J_{wd}(4 \times 0.2\,\mathrm{kg}$ at $r_{wd} = 0.05\,\mathrm{m})$	$0.0021\,\mathrm{kg\,m^2}$
$J_{wd}(4 \times 0.5\,\mathrm{kg}$ at $r_{wd} = 0.05\,\mathrm{m})$	$0.00561\,\mathrm{kg\,m^2}$
$J_{wl}(4 \times 0.2\,\mathrm{kg}$ at $r_{wd} = 0.1\,\mathrm{m})$	$0.00824\,\mathrm{kg\,m^2}$
$J_{wl}(4 \times 0.5\,\mathrm{kg}$ at $r_{wd} = 0.1\,\mathrm{m})$	$0.0206\,\mathrm{kg\,m^2}$
$J_{pd}(n_{pd} = 24)$ or $J_{pl}(n_{pl} = 24)$	$0.000008\,\mathrm{kg\,m^2}$
$J_{pd}(n_{pd} = 36)$ or $J_{pl}(n_{pl} = 36)$	$0.000039\,\mathrm{kg\,m^2}$
c_1	$0.004\,\mathrm{Nm/rad/s}$
c_2	$0.05\,\mathrm{Nm/rad/s}$
k	$8.45\,\mathrm{Nm/rad}$

4 Control Solutions for Driving Systems with BLDC-m and DC-m

4.1 Cascade Control of the Electric Drive (Servo-Drive) for a HEV

Controller Design. Two control solutions are presented for the HEV application presented in Section 3.2, Both solutions have two control loops in a CCS [9, 52] which differs in external control loop (vehicle speed ω):

1. CCS with a classical PI controller, Fig. 20, and
2. CCS with a 2-DOF PI controller, Fig. 21, which includes a forcing block to correct the current reference for the inner loop; the effect of this is that the settling time of the system will decrease.

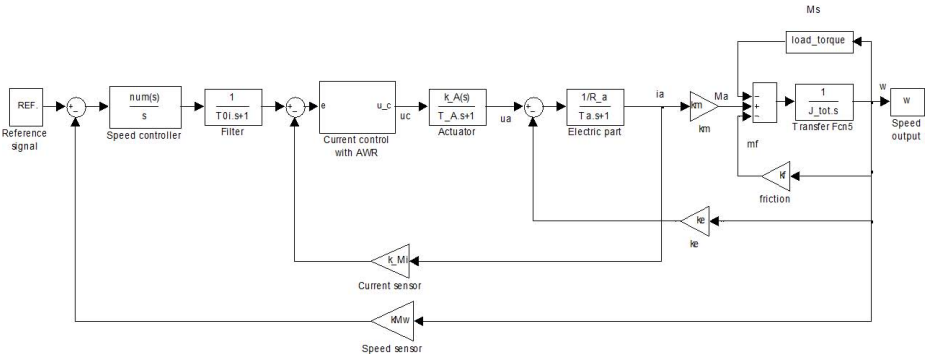

Fig. 20. Cascade control structure for the DC-m with PI controller

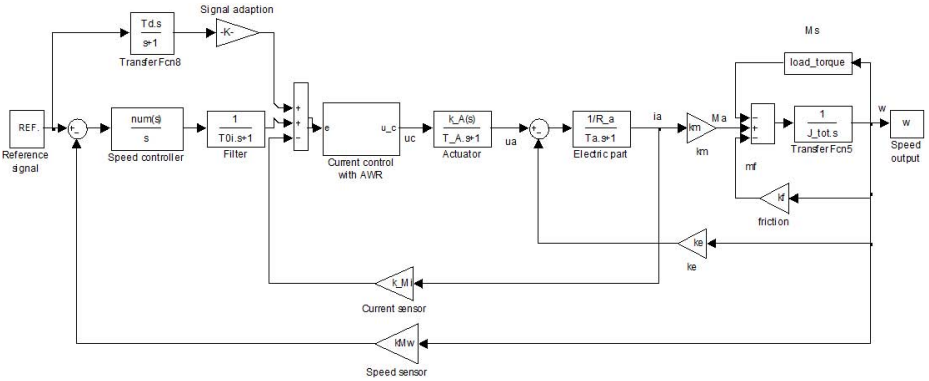

Fig. 21. Cascade control structure for the DC-m: speed control with reference forcing block

The inner control loop consists of a PI controller with AWR measure; the con-troller parameters were calculated based on the MO-m having the design relation (33) [11]:

$$H_{Cc}(s) = \frac{k_{ci}}{s}\left(1 + sT_{ci}\right), \quad K_{ci} = \frac{1}{2k_{pi}T_{\Sigma i}}, \quad T_{ci} = T_a. \tag{35}$$

The controller parameters results as $k_{ci} \approx 7$ and $T_{ci} = 0.1\,\mathrm{s}$. The AWR measure was introduced to attenuate the effects of going into limitation of the controller; other methods for handling the constraints in the control signal can also be used.

Neglecting the friction coefficient in the plant, k_f, for a simplified design of the speed controller for the plant a simplified t.f. can be considered:

$$H_p(s) = \frac{k_p}{s\,(1 + sT_{\Sigma\omega})}, \tag{36}$$

where $T_{\Sigma\omega} \approx 2T_{\Sigma\omega} + T_{i0}$ stands for the current loop and parasitic time constants ($T_{i0} \approx 0.05\,\mathrm{s}$), k_p characterizes the dynamics of the mechanical part of the driving system (J_{tot}), the inverse of the current sensor k_{Mi} and the speed sensor $k_{M\omega}$. So, the speed controller is of PI type having the parameters $k_{c\omega} \approx 35.0$ and $T_{c\omega} = 1.75\,\mathrm{s}$.

For the second case the controller is the same and the feed forward correction term is a Derivative with first order Lag type filter (DL1) with the t.f.

$$H_{ff}(s) = \frac{56s}{1 + s}. \tag{37}$$

Simulation Results and Interpretation. The considered simulation scenario is part from the urban part of the NEDC (New European Drive Cycle) used in testing vehicle's HEV (more generally, EV) consumption [9], consisting in an acceleration part, a part with constant velocity and a part of deceleration until a stop is reached. The load of the system is taken into account by means of (25)–(27) [49, 52]. Both CS behaviours are simulated and the comparison of the currents and dynamics is performed. Sensitivity aspects for a change in the mass of the plant are also treated in [9]. The registered variables are: the velocity (speed), the current and the electromagnetic torque M_a vs. disturbance torque M_s.

- *The case of simple CCS with PI controller.* The simulation results are depicted in Figs. 22, 23 and 24.
- *The case of CCS with correction in the current reference, the 2-DOF-PI solu-tion.* The differences in the speed are insignificant. So the differences in the current behaviour between the solutions are depicted, together with the active power (dashed line – simple cascade structure, solid line – structure with current correction), Figs. 25 and 26. It can be remarked that the active differences in the consumed energy (power) are proportional with the current.

- *The simple cascade structure with modified load.* The presented simulation refers the case when the mass of the vehicle is changed with +25% of it

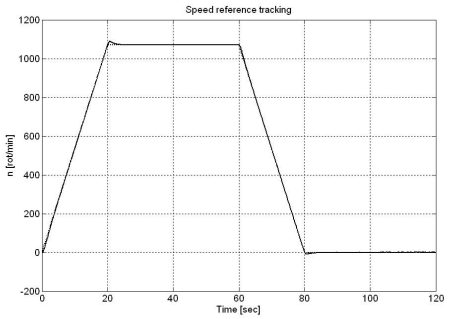

Fig. 22. Speed reference tracking

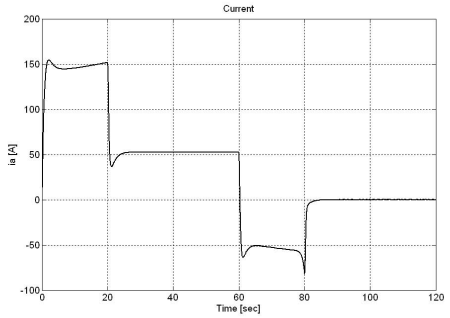

Fig. 23. Current response

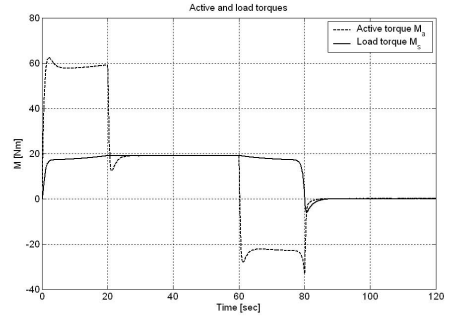

Fig. 24. Active torque M_a versus disturbance torque M_s

(solid line – original load, dashed line – increased load): $m_{\text{veh}} = m_{\text{veh0}} + \Delta m$, resulting $m_{\text{veh}} = 2332\,\text{kg}$. The simulations are presented in Figs. 27 and 28 (for the first cascade structure). Other cases are presented and discussed in detail in [9].

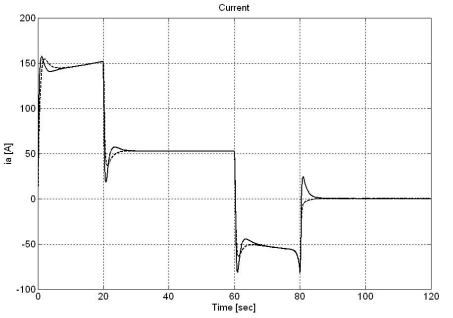

Fig. 25. Comparison of the currents

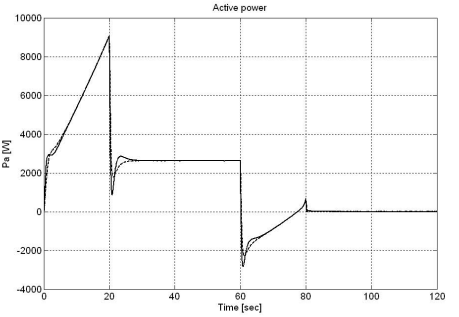

Fig. 26. Comparison of the active powers

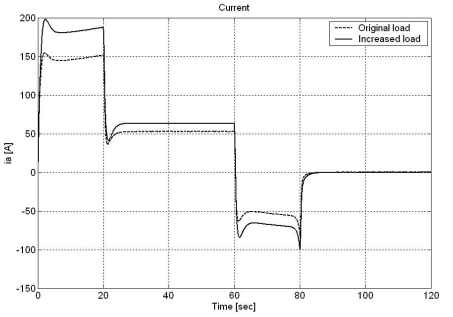

Fig. 27. Behaviour of the current

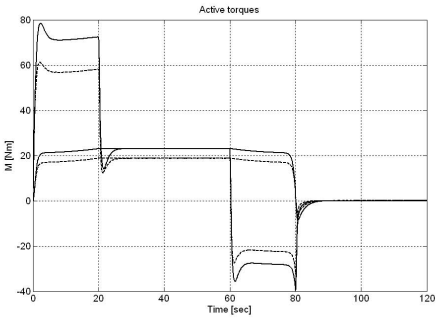

Fig. 28. Active torque M_a vs. disturbance torque M_s

The simulated cases reflect a very good behaviour of the CSs regarding reference tracking, disturbance rejection and also low sensitivity to parameter changes. More then, test simulation extended for the NEDC confirm the summarised results. Alternative solutions can be the GPC and different adaptive and variable structure controller solutions presented in Section 2 and in [9, 50, 54, 55].

4.2 Control Solution for the Electric Drive with BLDC-m and DC-m with VMI (the Winding System)

The DC-m drive with VMI in the simulated case. The cascade control structure (CCS) with PI(D) Speed Controller with Bump-less Switching for the speed controller is presented in Fig. 1. Due to the fact that the application has continuously variable parameters in a large domain, the control solution with bump-less switching of the c.a. is a good and practical option.

The development of the speed controller was considered in the context of Section 2 as follows:

1. in its classical PI controller (as the basic case);
2. an extension for a fuzzy PI Takagi-Sugeno Fuzzy controller;
3. a PI Quasi-Relay Sliding Mode Controller and
4. a Neuro-Fuzzy Controller.

All solutions are based on the locally linearised MMs. The "best controller-plant combinations" are summarized (dashed) in Table 6 after testing on laboratory equipment [53]. The most favourable case analysis is conducted in [60].

The basic CCS with discrete-time PI control algorithm. For the winding system the controller switching between PI c.a. (Figs. 1 and 2). Depending on the

Table 6. Combination between plant parameters and controller parameters

	r_0/J_0	$r_{\text{med}}/J_{\text{med}}$	$r_{\max}/J_{\max}$
C-1-ω Optimal for r_0	Case study 1.1 $r_0, Cr_0 - \omega$	Case study 1.2 $r_{\text{med}}, Cr_0 - \omega$	Case study 1.3 $r_{\max}, Cr_0 - \omega$
C-2-ω Optimal for r_{med}	Case study 2.1 $r_0, Cr_{\text{med}} - \omega$	Case study 2.2 $r_{\text{med}}, Cr_{\text{med}} - \omega$	Case study 2.3 $r_{\max}, Cr_{\text{med}} - \omega$
C-3-ω Optimal for $r_{\max}$	Case study 3.1 $r_0, Cr_{\max} - \omega$	Case study 3.2 $r_{\text{med}}, Cr_{\max} - \omega$	Case study 3.3 $r_{\max}, Cr_{\max} - \omega$

imposed performances the c.a.s can be designed using the MO-m, the ESO-m or the 2p-SO-m; the switching structure presented in Figs. 1 and 2 was applied without difficulties. The calculated values for the controller parameters (for the speed controller, the dashed cases) are synthesized in Table 7.

Table 7. Controller parameters (for the PI c.a.)

Controller type	The values for the parameters					
	k_C	T_i	q_{0pi}	q_{1pi}	p_{0pi}	p_{1pi}
0	1	2	3	4	5	6
C-i_a	0.5	0.0333	0.5019	−0.4981	1	−1
C-1-ω_{11}	0.1	0.125	0.1001	−0.0999	1	−1
C-2-ω_{22}	0.055	0.0688	0.0551	−0.0549	1	−1
C-3-ω_{33}	0.0025	0.0031	0.0026	−0.0024	1	−1

The Takagi-Sugeno PI Fuzzy Controllers. The Takagi-Sugeno PI (TS-PI-FC) quasi-continuous fuzzy controller structure (TS-PI-FC) with OI was adopted based on the continuous-time PI controller solution. The algorithm is modelled by the recurrent equations with variable parameters. Finally this leads to the PI quasi-continuous digital controller with OI (11), [58] (based on [34] other alternative solution can be done). The bump-less transfer of the command is structural ensured by the TS-FC. The expressions of the control algorithms are given by relation (11).

The PI Quasi-Relay Sliding Mode Controller. The block diagram of the PI quasi relay sliding mode controller – in its classical structure – is presented in Fig. 12. The fuzzy-block of the controller is defined using the principles synthesized in [61]: for the inputs in the nonlinear FC block three linguistic terms are used (with triangular and trapezoidal form, TL_{ek} and $TL_{\Delta ek} \in \{N, ZE, P\}$, $B_e = 13$

and $h = 0.00025\,\mathrm{s}$; the inference engine use the SUM and PROD operators and the rule base is a complete one defined by 9 rules

$$\begin{aligned}
&\text{IF } e_k \text{ IS } N \text{ AND } \Delta e_k \text{ IS } P \text{ THEN } \Delta u_k = K_{p1}\left[\Delta e_k + \alpha_1 e_k\right],\\
&\text{IF } e_k \text{ IS } Z \text{ AND } \Delta e_k \text{ IS } P \text{ THEN } \Delta u_k = K_{p2}\left[\Delta e_k + \alpha_2 e_k\right],\\
&\text{IF } e_k \text{ IS } P \text{ AND } \Delta e_k \text{ IS } P \text{ THEN } \Delta u_k = K_{p3}\left[\Delta e_k + \alpha_3 e_k\right],\\
&\text{IF } e_k \text{ IS } N \text{ AND } \Delta e_k \text{ IS } Z \text{ THEN } \Delta u_k = K_{p4}\left[\Delta e_k + \alpha_4 e_k\right],\\
&\text{IF } e_k \text{ IS } Z \text{ AND } \Delta e_k \text{ IS } Z \text{ THEN } \Delta u_k = K_{p5}\left[\Delta e_k + \alpha_5 e_k\right],\\
&\text{IF } e_k \text{ IS } P \text{ AND } \Delta e_k \text{ IS } Z \text{ THEN } \Delta u_k = K_{p6}\left[\Delta e_k + \alpha_6 e_k\right],\\
&\text{IF } e_k \text{ IS } N \text{ AND } \Delta e_k \text{ IS } N \text{ THEN } \Delta u_k = K_{p7}\left[\Delta e_k + \alpha_7 e_k\right],\\
&\text{IF } e_k \text{ IS } Z \text{ AND } \Delta e_k \text{ IS } N \text{ THEN } \Delta u_k = K_{p8}\left[\Delta e_k + \alpha_8 e_k\right],\\
&\text{IF } e_k \text{ IS } P \text{ AND } \Delta e_k \text{ IS } N \text{ THEN } \Delta u_k = K_{p9}\left[\Delta e_k + \alpha_9 e_k\right].
\end{aligned} \tag{38}$$

The parameters of the digital control algorithms are

$$\begin{aligned}
&u_{jk} = u_{j,k-1} - K_{Pi}^{(j)}\left[\left(1-\alpha_i^{(j)}\right)e_{jk} - e_{j,k-1}\right], \qquad j = 1,\ldots,9,\\
&e_{jk} = w_k - y_k = e_k, \qquad j = 1,2,3 \text{ for the c.a.}(j).
\end{aligned} \tag{39}$$

The Hybrid Neuro-Fuzzy Takagi-Sugeno quasi PI Controller (T-S PI-N-FC). The CS structure is presented in Fig. 29. The reference model (MR) is a PL2 block ($b_2 = b_1 = 0$, $b_0 = 1$; $a_2 = T_{\mathrm{imp}}^2$, $a_1 = 2\zeta_{\mathrm{imp}}T_{\mathrm{imp}}$, $a_0 = 1$ with $\zeta_{\mathrm{imp}} = 1$, $T_{\mathrm{imp}} = 1$), having the discrete equivalent in form

$$\begin{aligned}
&y_{m,k} = -d_1 y_{m,k-1} - d_2 y_{m,k-2} - c_0 r_k + c_1 r_{k-1} + c_2 r_{k-2},\\
&c_0 = -\frac{h^2}{\left(h+2T_{\mathrm{imp}}\right)^2}, \quad c_1 = \frac{2h^2}{\left(h+2T_{\mathrm{imp}}\right)^2}, \quad c_2 = \frac{h^2}{\left(h+2T_{\mathrm{imp}}\right)^2},\\
&d_1 = \frac{2\left(h^2 - 4T_{\mathrm{imp}}^2\right)}{\left(h+2T_{\mathrm{imp}}\right)^2}, \quad d_2 = \frac{\left(h-4T_{\mathrm{imp}}\right)^2}{\left(h+2T_{\mathrm{imp}}\right)^2}.
\end{aligned} \tag{40}$$

The adaptation block BA modifies the rule base of the FC. The parameters of the speed controllers are the same as those given in Table 7, the differences are provided by the tuning parameters $\{B_e, B_{\Delta e}, B_{\Delta u}\}$ for the TS-PI-FC and by the parameters $\{B_e, B_{eI}, B_u\}$ for the hybrid T-S PI-N-FC [33, 63].

Simulation results. From the simulation results synthesized in [33] and in Figs. 30(a)–(c), 31(a)–(c) and 32(a)–(c) illustrate suggestively that the CS-s ensure good behaviours as good tracking, small overshoots and settling times. The two fuzzy control systems – the TS-PI-FC with output integration and the T-S PI-N-FC – ensure improved performance compared to the linear control system. The implementation of the hybrid T-S PI-N-FC on a BLDC-m based servo system with a similar benchmark MM leads to good experimental results [33].

Figs. 31(a)–(c) and Figs. 32(a)–(c) illustrate that the best performances are provided by case study 1.1, case study 2.2 and case study 3.3.

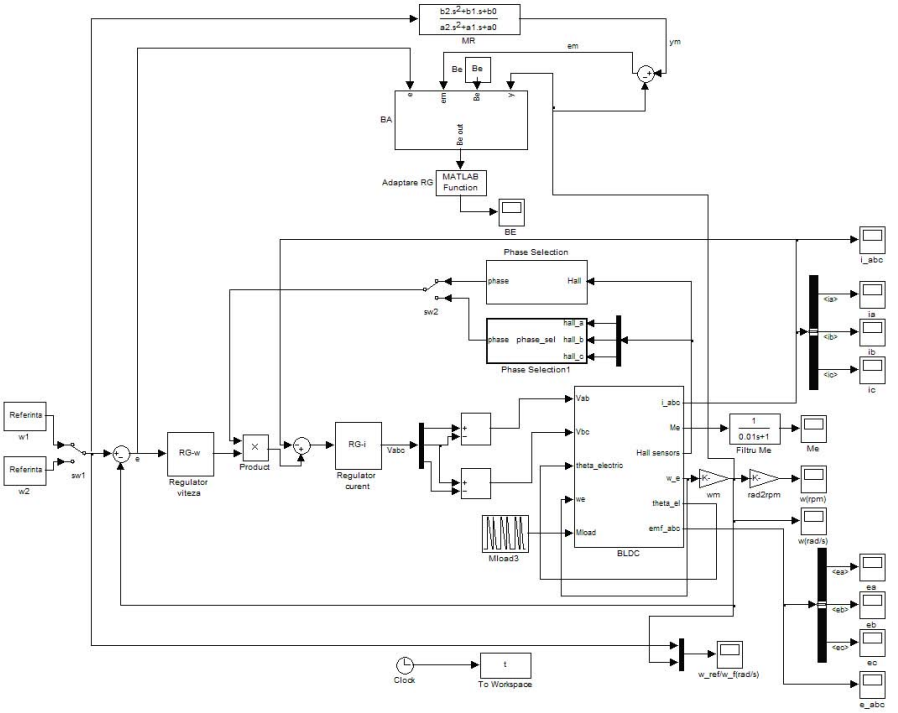

Fig. 29. Block diagram of the Hybrid Neuro-Fuzzy Takagi-Sugeno quasi PI Controller

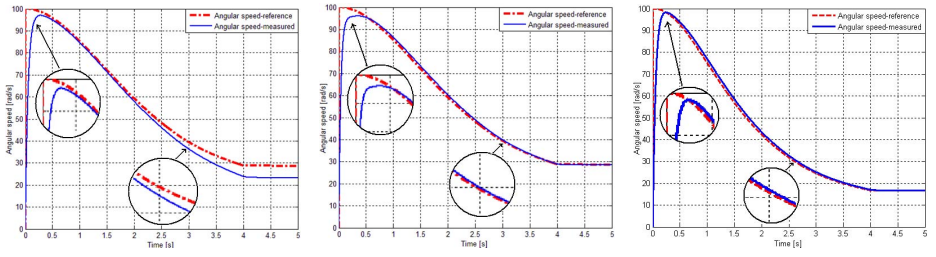

Fig. 30. Simulation results for (a) linear, (b) fuzzy and (c) neuro-fuzzy CS for DC-m based servo system with VMI: angular speed (reference input and measured angular speed) versus time

The Model 220 Industrial Plant Emulator (M 220 IPE) (electric drive with BLDC-m). Experiments and simulations have been conducted for the M 220 IPE application [33] using the details described in Sections 3.1 and 3.3.d, for different equipment facilities, different CSs, different inputs and different operating scenarios. Only the case of rigid transmission is treated to assess the main control performance.

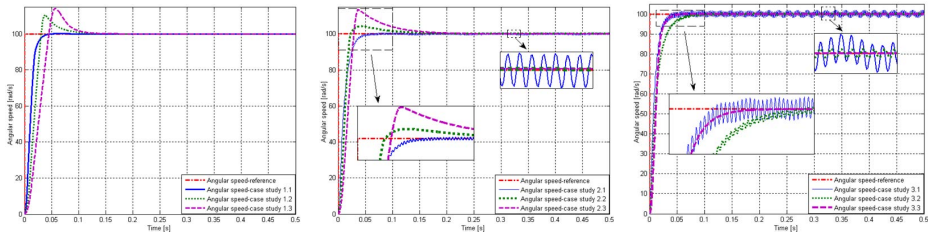

Fig. 31. Simulation results for fuzzy control system (TS-PI-FC with OI) of DC m based servo: (a) angular speed versus time (b) angular speed versus time (cases 2.1–2.3),(c) angular speed versus time (cases 3.1–3.3)

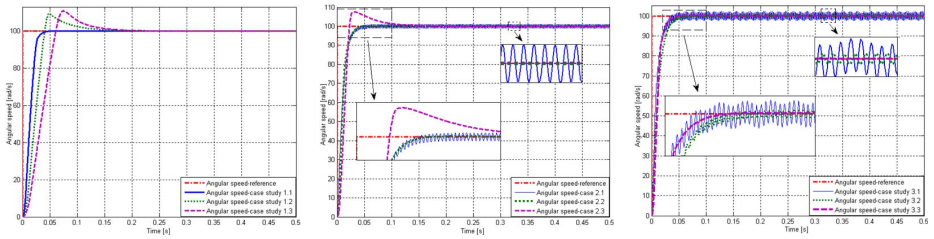

Fig. 32. Simulation results for neuro-fuzzy control system (T-S PI-N-FC) of DC-motor based servo (cases 3.1-3.3): (a) angular speed versus time (b) angular speed versus time (c) angular speed versus time

The developed CCS. Figs. 33, 34 and 35 illustrate the main four control structures. Due to a particularity in the equipment (software) the implementation of the natural PI controller must be extended with a serial PDL1 filter. Therefore, each case results in real PID controllers.

– The CCS with external PI(D) controller, the basic solution, presented in Fig. 33. The controller's t.f. and the values for the parameters calculated with the ESO-m for $\beta = 9$ are

$$H_{\text{PID-C}} = \frac{k_r}{s}\left(1 + sT_r\right)\left(1 + sT_r'\right), \qquad k_r = 0.001, \qquad T_r = 0.05\,\text{s}, \qquad T_r' = 1.95\,\text{s}. \tag{41}$$

– The CCS with classical 2-DOF control solution, presented in Fig. 34. The values of the parameters of the controller's t.f. are given in Table 8.
– The CCS with sliding-mode PI-D controller solution, presented in Fig. 35. The parameters of the controllers have been calculated, and they are synthesized in Table 9.
– The CCS with Takagi-Sugeno FC solution with PD+I controller, Fig. 36. The parameters of the controllers have been calculated, and they are synthesized in Table 10.

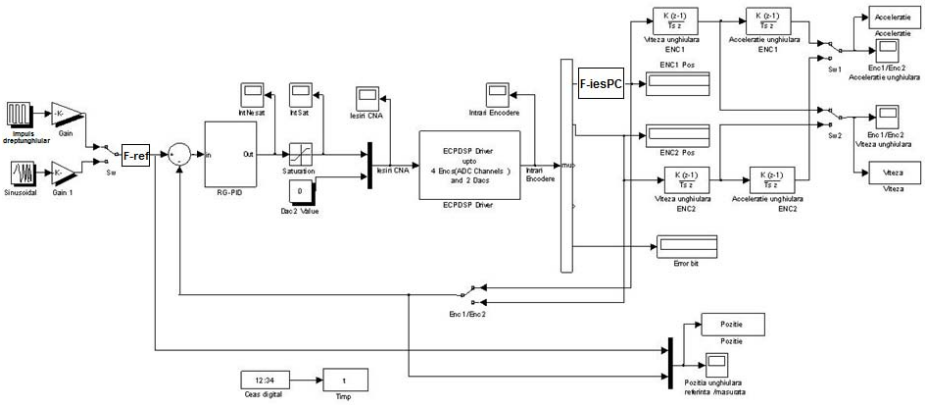

Fig. 33. The CCS with external PI(D) as the basic control solution

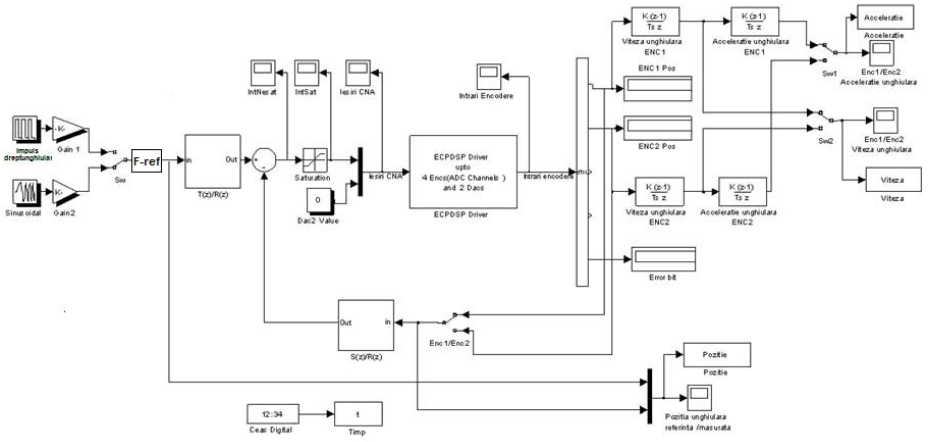

Fig. 34. The CCS with external classical 2-DOF control solution

Table 8. The values of the polynomials $R\left(z^{-1}\right)$, $S\left(z^{-1}\right)$ and $T\left(z^{-1}\right)$

$R\left(z^{-1}\right)$			$S\left(z^{-1}\right)$			$T\left(z^{-1}\right)$		
r_0	r_1	r_2	s_0	s_1	s_2	t_0	t_1	t_2
0.028	−0.040	0.012	0.049	−0.094	0.045	0.042	−0.08	0.038

– The CCS with 2-DOF Takagi-Sugeno FC solution with PD+I as main controller and filters blocks on the reference and feedback channel, Fig. 37. The values of the controller's parameters are synthesized in Table 11.

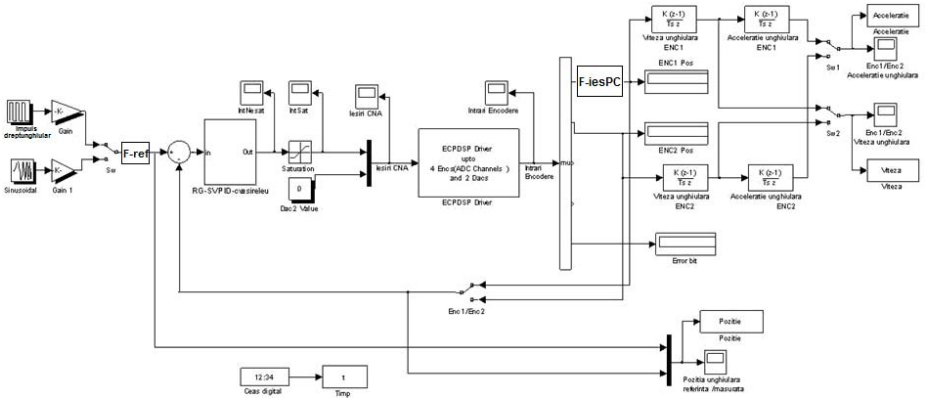

Fig. 35. The CCS with sliding-mode PI-D controller

Table 9. The values of the controller's parameters

Sliding mode parameters		PID controller, $H_{\text{RG-PID}}$					
c	α	K_p	K_i	K_d	k_r	T_r	T_r'
1	2	3	4	5	6	7	8
10000	1.75	0.2	0.1	0.01	0.1	0.05	1.95

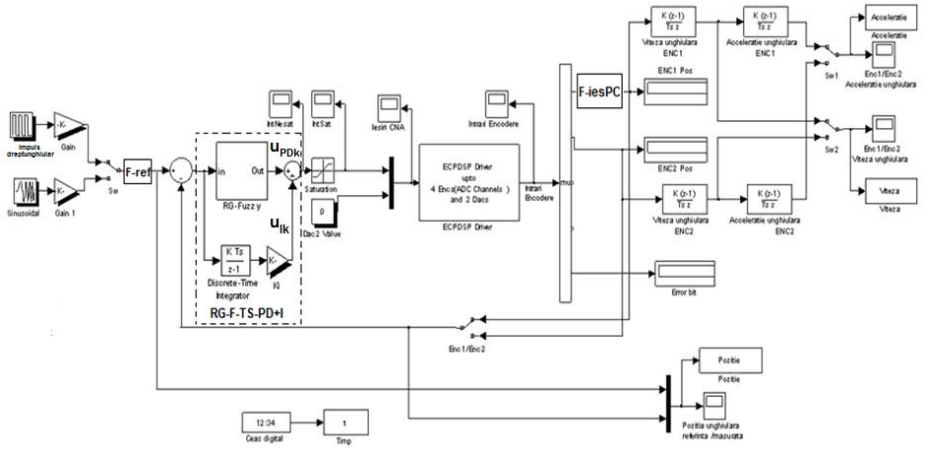

Fig. 36. The CCS with Takagi-Sugeno FC solution with PD+I controller

Simulation results. The solutions were tested as positioning CS so the input reference was an angular position [33]. All solutions gives good control performances; the best results are given by the 2-DOF Takagi-Sugeno FC solution with PD+I as main controller and filters blocks on the reference and feedback channel.

Table 10. The values of the controller's parameters

Ccontroller parameters					
K_p	K_i	K_d	k_1	k_2	α
0.2	0.1	0.01	2.5	0.2	0.08

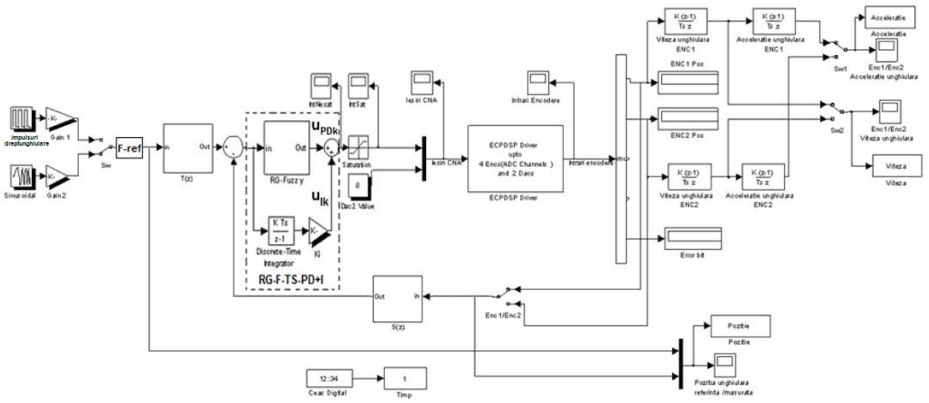

Fig. 37. The CCS with 2-DOF Takagi-Sugeno FC solution with PD+I controller

Table 11. The values of the controller's parameters

2-DOf controller						TS-FC with PD+I controller			
$T\left(z^{-1}\right)$			$S\left(z^{-1}\right)$			RG-F-TS-PD			I
t_0	t_1	t_2	s_0	s_1	s_2	k_1	k_2	α	K_i
0.042	−0.08	0.038	0.049	−0.094	0.045	2.5	0.2	0.08	0.1

5 Conclusions

Using some practical development methods which can be implemented as LCA solutions, this chapter has synthesized some pragmatic control solution, dedicated to plants working under continuously variable conditions: variable plant parameters or (the worst case) variable structure, variable reference and variable load (disturbance). From a large case of such applications, two speed control applications, namely with DC-m and with BLDC-m, have been treated: a case specific to the metallurgical industry and the speed control of an electric (hybrid) vehicle model. The efficiency of the algorithms has been tested and illustrated on different plant models and also on laboratory equipment with variable moment of inertia. The presented algorithms are easily adaptable to similar applications. Several fuzzy and nonlinear elements can be incorporated [64–70, 70, 72–74].

Acknowledgments. This work was supported by a grant of the Romanian National Authority for Scientific Research, CNCS – UEFISCDI, project number PN-II-ID-PCE-2011-3-0109. Also, the work was partially supported by the strategic grants POSDRU 6/1.5/S/13 (2008) and POSDRU ID 77265 (2010) of the Ministry of Labour, Family and Social Protection, Romania, co-financed by the European Social Fund – Investing in People.

Main abbreviations

AWR	Anti-Windup Reset	1-DOF	one Degree of Freedom
MBC	Model-Based Control	2-DOF	two Degree of Freedom
MM	Mathematical Model	FC	Fuzzy Controller
EV	Electric Vehicle	TS-FC	Takagi-Sugeno Fuzzy Controller
HEV	(Hybrid) Electric Vehicle	TS-PI(D)-FC	Takagi-Sugeno PI(D) Fuzzy Controller
VMI	Variable Moment of Inertia	OI	(with) output integration
BLDC-m	Brush-Less DC motor	II	(with) input integration
CS	Control Structure	P, I, D	the Proportional, Integral, Derivative components
CCS	Cascade Control Structure	L1, L2	first /second order filter with lag
c.a.	control algorithm	DP-CS	Dynamic Programming (based) Control Strategy
t.f.	transfer function	MPC	Model Predictive Control
MO-m	Modulus-Optimum method	GPC	Generalized Predictive Control
SO-m	Symmetrical Optimum method	ESO-m	Extended Symmetrical Optimum method
2-p-SO-m	double parameterization based Symmetrical Optimum method		

References

1. Christian, J.A., Turbe, M.A., Kabo, E.M., Manno, L.C., Johnson, E.N.: Development of a variable inertia reaction wheel system for spacecraft attitude control. In: Proceedings of AIAA Guidance, Navigation, and Control Conference and Exhibit, Providence, RI, USA, 13 p. (2004)
2. Akpolat, Z.H., Asher, G.M., Clare, J.C.: A practical approach to the design of robust speed controllers for machine drives. IEEE Trans. Ind. Electron. 47, 315–324 (2000)
3. Mink, F., Bahr, A.: Adaptive speed control for drives with variable moments of inertia and natural drequencies. LTi DRIVES GmbH Entwicklung Software, Lahnau, Germany (2011)
4. Lamar, K.: Digital control of permanent magnet synchronous motors. In: Proc. Budapest-Tech Jubilee Conference, Budapest, Hungary, pp. 213–228 (2004)

5. Modi, V.J., Karray, F., Mah, H.A.: Composite Control Scheme for Joint Tracking and Active Vibration Suppression of Mobile Flexible Manipulator Systems. Acta Astronautica 36, 261–275 (1995)
6. Crowder, R.M.: Electric Drives and their Controls. Oxford University Press Inc., New York (1998)
7. Rizzoni, G.: Priciples and Applications of Electrical Engineering. McGraw-Hill (2000)
8. Preitl, Z., Bauer, P., Bokor, J.: Fuel Consumption Optimization for Hybrid Solar Vehicle. In: Proc. Workshop on Hybrid Solar Vehicles, Salerno, Italy (2006)
9. Preitl, Z.: Control design methods for optimal energy consumption systems, PhD Thesis, Supervisors: Prof. Dr. József Bokor, member of The Hungarian Academy of Science, Budapest University of Technology and Economics (2009)
10. Ťapák, P., Huba, M., Žáková: Constrained Control for Systems with Relative Degree One. In: Proc. 17th IFAC World Congress, Seoul, South Korea, vol. 17, pp. 5814–5819 (2008)
11. Åström, K.J., Hägglund, T.: PID controller theory: Design and tuning. Instrument Society of America, Research Triangle Park, NC (1995)
12. Ozawa, S., Furuya, H.: Feedback Liniearization Technique in Variable Inertia Systems. Trans. Japan Soc. Aero Space Sci. 45(147), 1–9 (2002)
13. Möhler, R.R.: Applications to Bilinear Control. Prentice Hall, Englewood Cliffs (1991)
14. Sherer, C.: Mixed H_2/H_∞ Control. In: Trends in Control: An European Perspective, Volume of the Special Contributions to the ECC, pp. 173–216 (1995)
15. Chiali, M., Gahinet, P.: H_∞ Design with Pole Placement Constraints: an LMI Approach. IEEE Trans. Automat. Control 41, 358–367 (1996)
16. Åström, K.J., Panagopoulos, H., Hägglund, T.: Design of PI controllers based nonconvex optimization. Automatica 34, 585–601 (1998)
17. Preitl, S., Precup, R.-E.: Extension of tuning relations after symmetrical optimum method for PI and PID controllers. Automatica 35(10), 1731–1736 (1999)
18. Preitl, S., Precup, R.-E.: Linear and Fuzzy Control Extensions of the Symmetrical Optimum Method. In: Proc. International Conference on Complex Systems: Synergy of Control, Computing & Communications (COSY 2011), Ohrid, Republic of Machedonia, pp. 59–68 (2011)
19. Vrancic, D., Peng, Y., Strmcnik, S.: A new PID controller tuning method based on multiple integrations. Control Engineering Practice 7(5), 623–633 (1999)
20. Vrancic, D., Strmcnik, S., Juricic, D.: A magnitude optimum multiple integration tuning method for filtered PID controller. Automatica 37(9), 1473–1479 (2001)
21. Papadopoulos, K.G., Mermikli, K., Margaris, N.I.: Optimal tuning of PID controllers for integrating processes via the symmetrical optimum criterion. In: Proc. 19th Mediterranean Conference on Control and Automation (MED 2012), Corfu, Greece, pp. 1289–1294 (2011)
22. Papadopoulos, K.G., Mermikli, K., Margaris, N.I.: On the automatic tuning of PID type controllers via the magnitude optimum criterion. In: Proc. 2012 IEEE International Conference on Industrial Technology (ICIT 2012), Athens, Greece, pp. 869–874 (2012)
23. Papadopoulos, K.G., Margaris, N.I.: Extending the symmetrical optimum criterion to the design of PID type-p control loops. Journal of Process Control 22(1), 11–25 (2012)
24. Loron, L.: Tuning of PID controllers by the non-symmetrical optimum method. Automatica 33(1), 103–107 (1997)

25. Precup, R.-E., Preitl, S.: Development of some fuzzy controllers with non-homogenous dynamics with respect to the input channels meant for a class of systems. In: Proc. European Control Conference (ECC 1999), Karlsruhe, Germany, paper index F56, 6 p. (1999)
26. Araki, M., Taguchi, H.: Two-degree-of-freedom PID controllers. Int. J. Control Automat. Syst. 1, 401–411 (2003)
27. Preitl, Z.: Model Based Design Methods for Speed Control, Applications. PhD Thesis, "Politehnica" University of Timisoara, Editura Politehnica, Timisoara, Romania (2008)
28. Preitl, S., Precup, R.-E., Preitl, Z.: Aspects concerning the tuning of 2-DOF fuzzy controllers. In: Proc. Xth Triennial International SAUM Conference on Systems, Automatic Control and Measurements (SAUM 2010), Nis, Serbia, pp. 210–219 (2010)
29. Miklosovic, R., Gao, Z.: A robust two-Degree of Freedom control design Technique and its practical application. In: Proc. 39th IAS Annual Meeting Conference Record of the 2004 IEEE Industry Application Conference, vol. 3, pp. 1495–1502 (2004)
30. Preitl, S., Precup, R.-E., Dragos, C.-A., Radac, M.-B.: Tuning of 2-DOF fuzzy PI(D) controllers, laboratory applications. In: Proc. 11th International Conference on Computational Intelligence and Informatics (CINTI 2010), Budapest, Hungary, pp. 237–242 (2010)
31. Bagheri, P., Nemati, H.: Novel tuning strategy for two-degree-of-freedom PI controllers. In: Proc. 18th IFAC World Congress, Milano, Italy, pp. 6757–6762 (2011)
32. Preitl, Z., Levendovszky, T.: Computer Aided Design of Two-Degree-of-Freedom (2DOF) Controllers. Buletinul Stiintific al Universitatii "Politehnica" din Timisoara, Romania, Seria Automatica si Calculatoare 48(62), 70–75 (2003)
33. Stinean, A.-I.: Contribuţii la Dezvoltarea unor Soluţii de Reglare Dedicate Sistemelor de Actionare Electrică cu Parametri Variabili si cu Intrări Variabile in Timp. Ph.D. thesis, Politehnica University of Timisoara, Timisoara, Romania (2014) (in Romanian)
34. Precup, R.-E., Preitl, S.: Fuzzy Controllers. Editura Orizonturi Universitare, Timisoara (1999)
35. Stinean, A.-I., Preitl, S., Precup, R.-E., Dragos, C.-A., Radac, M.-B.: Classical and Fuzzy Approaches to 2-DOF Control Solutions for BLDC-m Drives. In: Pap, E. (ed.) Intelligent Systems: Models and Applications. TIEI, vol. 3, pp. 175–193. Springer, Heidelberg (2013)
36. Proceedings of 18th IFAC World Congress, Milan, Italy (2011)
37. Bay, O.F., Bal, G., Demirbas, S.: Fuzzy Logic Based Control of a Brushless DC Servo Motor Drive. In: Proc. 7th International Power Electronics & Motion Control Conference Exhibition (1996), Budapest, Hungary, vol. 3, pp. 448–452 (1996)
38. Lomonova, E.A., Miziurin, S.R., Klaassens, J.B.: Brushless Machines as Electromechanical Actuators for Flight Control Systems. In: Proc. 7th International Power Electronics & Motion Control Conference Exhibition, Budapest, Hungary, vol. 2, pp. 627–631 (1996)
39. Vaščák, J., Madarász, L.: Adaptation of fuzzy cognitive maps - a comparison study. Acta Polytechnica Hungarica 7, 109–122 (2010)
40. Preitl, S., Precup, R.-E., Preitl, Z.: Control structures and algorithms, vol. 1, 2. Editura Orizonturi Universitare, Timisoara (2009) (in Romanian)
41. Cao, W., Yeng, C.S., Chakravarthy, V.K.: An integrated nonlinear observer with sliding mode estimation for a class of nonlinear uncertain systems. In: Proc. 42nd IEEE Conference on Decision and Control, pp. 5741–5746 (2003)

42. Zhang, J., Shi, P., Xia, Y.: Robust adaptive sliding-mode control for fuzzy systems with mismatched uncertainties. IEEE Trans. Fuzzy Syst. 18, 700–711 (2010)
43. Utkin, V., Guldner, J., Shi, J.: Sliding Mode Control in Electro-mechanical Systems. CRC Press, Boca Raton (2009)
44. Baldursson, S.: BLDC motor modelling and control - A Matlab/Simulink implementation. M.Sc. Thesis, Institutionen för Energi och Miljö, Göteborg, Sweden (2005)
45. Nasar, S.A., Boldea, I.: Electric Drives, 2nd edn. CRC Press (2005)
46. Dixon, J.W., Real, I.: Current control strategy for brushless dc motors based on a common DC signal. IEEE Trans. Power Electron. 17, 232–240 (2002)
47. Yasuhiko, D.: Servo Motor and Motion control Using Digital Signal Processors, Texas Instruments. Prentice Hall, Englewood Cliffs (1990)
48. Bauer, P., Preitl, Z., Gaspar, P., Szabo, Z., Bokor, J.: Modelling of a Series Hybrid Electric Vehicle. In: Workshop on Hybrid Electric Vehicle Modelling and Control, Istanbul, Turkey (2007)
49. Preitl, Z., Kulcsár, B., Bokor, J.: Mathematical Models of a Hybrid Electric Vehicles. In: Proc. 8th International Conference on Technical Informatics (CONTI 2008), Timisoara, Romania, 6 p. (2008)
50. Tsai, T.-C., Tsai, M.-C.: Power Control of a Brushless Permanent Magnet Electric Machine for Exercise Bikes. In: Proc. 15th IFAC Triennial World Congress, Barcelona, Spain, 6 p. (2002)
51. Workshop Papers, Workshop on Hybrid Solar Vehicles, Salerno, Italy (2006)
52. Preitl, Z., Bauer, P., Bokor, J.: Cascade control solution for traction motor for hybrid electric vehicles. Acta Polytechnica Hungarica 4(3), 75–88 (2007)
53. ECP M 220, Industrial emulator/servo trainer model 220 system, testbed for practical control training, Bell Canyon, CA, USA. Educational Control Products (2010)
54. Musardo, C., Rizzoni, C., Guezennec, Y., Staccia, B.: A-ECMS: An Adaptive Algorithm for Hybrid Electric Vehicle Energy Management. European Journal of Control 11, 509–524 (2005)
55. Tsai, T.-C., Tsai, M.-C.: Power Control of a Brushless Permanent Magnet Electric Machine for Exercise Bikes. In: Proc. 15th IFACT Triennial World Congress, Barcelona, Spain (2002)
56. Precup, R.-E., Preitl, S.: On a hybrid PI-neuro-fuzzy controller meant for a class of non-minimum phase systems. In: Proc. 7th European Congress on Intelligent Technologies and Soft Computing (EUFIT 1999), Aachen, Germany, 6 p. (1999)
57. Precup, R.-E., David, R.-C., Petriu, E.-M., Rădac, M.-B., Preitl, S., Fodor, J.: Evolutionary optimization-based tuning of low-cost fuzzy controllers for servo systems. Knowledge-Based Systems 38, 74–84 (2013)
58. Stînean, A.-I., Preitl, S., Precup, R.-E., Dragoş, C.-A., Rădac, M.-B., Crainic, M.: Adaptable fuzzy control solutions for driving systems working under continuously variable conditions. In: Proc. 14th IEEE International Symposium on Computational Intelligence and Informatics (CINTI 2013), Budapest, Hungary, pp. 231–237 (2013)
59. Preitl, S., Stinean, A.-I., Precup, R.-E., Preitl, Z., Petriu, E.-M., Drago, C.-A., Rădac, M.-B.: Controller design methods for driving systems based on extensions of symmetrical optimum method with DC and BLDC Motor Applications. In: Proc. IFAC Conference on Advances in PID Control (PID 2012), Brescia, Italy, pp. 264–269 (2012)

60. Stinean, A.-I., Preitl, S., Precup, R.-E., Dragos, C.-A., Petriu, E.M., Radac, M.-B.: Choosing a Proper Control structure for a mechatronic system with variable parameters. In: Proc. 2nd IFAC Workshop on Convergence of Information Technologies and Control Methods with Power Systems (ICPS 2013), Cluj-Napoca, Romania, pp. 29–34 (2013)
61. Precup, R.-E., Preitl, S.: On some low cost hybrid PI-neuro-fuzzy controllers for the second-order "right half plane zero" system. In: Proc. 13th CSCS Conference, pp. 170–175. Editura Politehnica Press, Bucharest (2001)
62. Stînean, A.-I., Preitl, S., Precup, R.-E., Petriu, E.-M., Dragoş, A.-C., Rădac, B.-M.: Solutions for avoiding the worst case scenario in driving system working under continuously variable conditions. In: Proc. IEEE 9th International Conference on Computational Cybernetics (ICCC 2013), Tihany, Hungary, pp. 339–344 (2013)
63. Stînean, A.-I., Preitl, S., Precup, R.-E., Dragoş, A.-C., Petriu, E.-M., Rădac, B.-M.: Low-Cost Neuro-Fuzzy Control Solution for Servo Systems with Variable Parameters. In: Proc. 2013 IEEE International Conference on Computational Intelligence and Virtual Environements for Measurement Systems and Applications (CIVEMSA 2013), Milano, Italy, pp. 156–161 (2013)
64. Precup, R.-E., Preitl, S.: Popov-type stability analysis method for fuzzy control systems. In: Proc. Fifth EUFIT 1997 European Congress, Aachen, Germany, pp. 1306–1310 (1997)
65. Carlsson, C., Fullér, R.: Optimization under fuzzy if-then rules. Fuzzy Sets and Systems 119(1), 111–120 (2001)
66. Baranyi, P., Tikk, D., Yam, Y., Patton, R.J.: From differential equations to PDC controller design via numerical transformation. Computers in Industry 51(3), 281–297 (2003)
67. Tar, J.K., Rudas, I.J., Bitó, J.F., Horváth, L., Kozlowski, K.: Analysis of the effect of backlash and joint acceleration measurement noise in the adaptive control of electro-mechanical systems. In: Proc. 2003 IEEE International Symposium on Industrial Electronics (ISIE 2003), Rio de Janeiro, Brazil, vol. 1, pp. 286–291 (2003)
68. Tanelli, M., Sartori, R., Savaresi, S.M.: Combining slip and deceleration control for brake-by-wire control systems: A sliding-mode approach. Eur. J. Control 13(6), 593–611 (2007)
69. Rudas, I.J., Fodor, J.: Intelligent systems. International Journal of Computers, Communications & Control 3, 132–138 (2008)
70. Blažič, S.: A novel trajectory-tracking control law for wheeled mobile robots. Robotics and Autonomous Systems 59(11), 1001–1007 (2011)
71. Tikk, D., Johanyák, Z.C., Kovács, S., Wong, K.W.: Fuzzy rule interpolation and extrapolation techniques: criteria and evaluation guidelines. Journal of Advanced Computational Intelligence and Intelligent Informatics 15(3), 254–263 (2011)
72. Angelov, P., Yager, R.: A new type of simplified fuzzy rule-based systems. International Journal of General Systems 41(2), 163–185 (2012)
73. Melin, P., Castillo, O.: A review on the applications of type-2 fuzzy logic in classification and pattern recognition. Expert Syst. Appl. 40(13), 5413–5423 (2013)
74. Petra, M.I., De Silva, L.C.: Implementation of folding architecture neural networks into an FPGA for an optimized inverse kinematics solution of a six-legged robot. International Journal of Artificial Intelligence 10(S13), 123–138 (2013)